THE JOURNAL OF PHYSICAL CHEMISTRY Letters

pubs.acs.org/JPCL Letter

Graphene Activation Explains the Enhanced Hydrogen Evolution on Graphene-Coated Molybdenum Carbide Electrocatalysts

Timothy T. Yang and Wissam A. Saidi*

Cite This: *J. Phys. Chem. Lett.* 2020, 11, 2759–2764 Read Online

ACCESS | Metrics & More | Article Recommendations | Supporting Information

ABSTRACT: Molybdenum carbides (Mo_xC) have shown high catalytic activities toward hydrogen evolution reaction (HER) when coupled with graphene. Herein, we use density functional theory (DFT) calculations in conjunction with *ab initio* thermodynamics and electrochemical modeling on γ-MoC supported graphene to determine the origin of the enhanced HER activities. In addition to previous claims that graphene's main role is to prevent agglomeration of Mo_xC nanoparticles, we show that the interplay between γ-MoC coupling and graphene defect chemistry activates graphene for the HER. For γ-MoC supported graphene systems, the HER mechanism follows the Volmer–Heyrovsky pathway with the Heyrovsky reaction as the rate-determining step. To simulate the electrochemical linear sweep voltammetry at the device level, we develop a computational current model purely from the thermodynamic and kinetics descriptors obtained using DFT. This model shows that γ-MoC supported graphene with divacancies is optimum for HER with an exchange current density of ~1×10^{-4} A/cm^2 and Tafel slope of ~50 mV/dec^{-1}, which are in good agreement with experimental results.

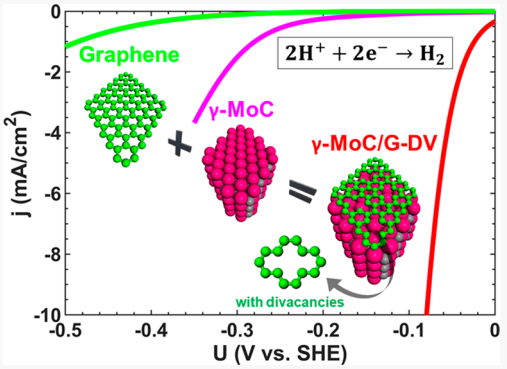

Water electrolysis is a promising approach for hydrogen production with no greenhouse gas emissions as long as renewable energy resources are used to drive water splitting. For this case, hydrogen is generated at the cathode site through hydrogen evolution reaction (HER). Despite the promise of molecular hydrogen for electrochemical energy storage and conversion, the high cost of the optimum catalyst, platinum, has been the bottleneck of wide-scale deployment for electrochemical hydrogen production.[1,2] Molybdenum carbide (Mo_xC) is an attractive catalyst for HER because of its low cost and high stability.[3,4] Recent studies have demonstrated a good HER catalytic activity of Mo_xC in various structures including nanowires,[5] microspheres,[6] hierarchically porous architecture,[7] or nano-octahedrons.[8] It is generally believed that Mo_2C phases such as β-Mo_2C exhibit excellent HER electrochemical catalytic behaviors[5,9] because their Mo–C mixed bands across the Fermi level provide a platinum-like metallic d-band structure.[10,11] On the other hand, MoC phases in hcp, fcc, or WC structure (γ-MoC) are less favored for catalytic activities owing to their covalent or mixed ionic–covalent characters.[3,10]

Several studies have shown that the catalytic activities of Mo_xC nanoparticles can be further enhanced by coupling to carbon-based materials.[12−18] To date, the main role of graphene in Mo_xC/graphene heterostructures is not clear. Because graphene is extremely inert to HER,[19] it is generally believed that graphene hinders the aggregation of Mo_xC nanoparticles, therefore maximizing the number of active sites.[6,8,15,17,20] However, previous studies showed that HER activities can also be induced at the interface of heterostructures[21−23] such as nitrogen-doped graphene/g-C_3N_4[24] and graphene/MoS_2.[19,25] This raises the question whether the coupling of graphene to Mo_xC functionalizes graphene toward HER. Moreover, if this is the case, then a fundamental understanding on the coupling behavior at the nanoscale can provide an opportunity to further enhance the HER activity.

Herein we use first-principles density functional theory (DFT) calculations in conjunction with *ab initio* thermodynamics and electrochemical methods to study the HER mechanism on γ-MoC supported graphene in acidic environments. Our main finding is that the coupling of graphene with γ-MoC induces new catalytic sites on graphene although graphene is inert in isolation. Further, we show that the HER activity of the coupled system is tunable with graphene defect chemistry, achieving an optimum value with divacancy defects. Thus, our studies suggest that the experimentally observed enhanced HER activity due to the coupling between Mo_xC nanoparticles and carbon-based materials[12−18,26] is not due to

Received: February 25, 2020
Accepted: March 18, 2020
Published: March 18, 2020

only preventing agglomeration of Mo_xC but is also due to an increase in the number of HER active sites. Further, to build a linkage with analytical electrochemistry, we use first-principles results to develop an electrochemical model for linear sweep voltammetry to quantify the HER activity under electrochemical conditions. This model shows that the exchange current density on the γ-MoC supported graphene with divacancy defects is at least 1×10^{-4} A/cm^2, which is comparable to experimental results and that of advanced HER catalysts.

We use the Vienna Ab Initio Simulation Package (VASP)[27,28] for the DFT calculations in conjunction with Perdew–Burke–Ernzerhof (PBE)[29] exchange–correlation functional and Tkatchenko–Scheffler[30,31] van der Waals corrections. The Zur and McGill scheme[32] is applied to build a supercell model for the heterostructure employing a small lattice misfit between γ-MoC Mo-terminated (001) and graphene. γ-MoC(001) termination is chosen as this is a stable termination with low surface energy.[4,10,33] The optimum interface structure was determined from the minimum of the potential energy surface constructed by shifting graphene with respect to the Mo- or C-terminated γ-MoC (001) and relaxing all atomic coordinates. Using this approach, we find that the Mo-terminated interface is the most stable with Mo sitting atop C sites of graphene. Using the same interface model, in addition to pristine graphene (MoC-G), we have investigated graphene with Stone–Wales (MoC-SW), monovacancy (MoC-MV), and divacancy (MoC-DV) defects. We find that graphene and γ-MoC (001) form a stable interface. The adhesion energies are relatively large and vary between −1.73 and −2.82 J/m^2 for graphene with or without defects (see the Supporting Information). We note that these defects can be controlled by chemical treatments and irradiation techniques.[34]

To study hydrogen adsorption on the surfaces, we use a single hydrogen atom to probe all possible adsorption sites to obtain the hydrogen adsorption energy

$$\Delta E_H = E_{H(n)} - E_{H(n-1)} - 0.5E_{H_2} \quad (1)$$

where $E_{H(n)}$ and $E_{H(n-1)}$ are the total energies of the system with n and $n-1$ adsorbed hydrogen H*, and E_{H_2} is the energy of H_2 molecule. Figure 1 shows ΔE_H on all the possible adsorption sites schematically. On MoC-G, H* is located only on atop C sites whereas hollow and bridge sites are unlikely to be occupied. For MoC-MV and MoC-DV, the most stable sites (ΔE_H = −0.3 and −0.7 eV) correspond to carbon atoms with dangling bonds. Also, on MoC-SW, a strong adsorption site (ΔE_H = −0.7 eV) appears at the apex of a pentagon carbon ring. In addition to the direct interaction of H* with C, the Mo d-band orbitals of subsurface Mo layers also affect hydrogen bonding. For example, on MoC-G, the ΔE_H of H* at the atop sites of C which is supported on top of subsurface Mo is about 1 eV weaker than that at C which is at Mo bridge sites. Overall, the filling sequence of these sites follows the adsorption strength: sites having strong interaction with H* are occupied first. This is similar to the β-Mo_2C surface as we have verified before.[35] Further, the induced-curvature of graphene due to its interaction with MoC causes sp^2–sp^3 hybridization also affects hydrogen adsorption strength,[36−38] which causes small variations of ΔE_H on some symmetric sites especially for MoC-DV.

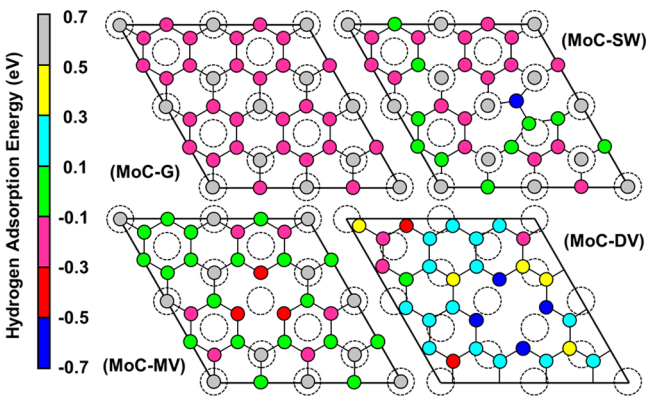

Figure 1. Hydrogen adsorption energies ΔE_H of the HER activation sites on γ-MoC supported graphene with graphene defects. The adsorption sites are located on atop sites of the carbon atoms of surface graphene. These surface carbon atoms are color coded to represent the hydrogen adsorption energy. The supporting sublayer Mo atoms of γ-MoC are shown as dashed circles.

We compute the hydrogen adsorption free energy ΔG_H (obtained from ΔE_H after adding phonon contributions, see the Supporting Information) to study HER thermodynamically. For $\Delta G_H > 0$, HER is endothermic while it is an exothermic process for $\Delta G_H < 0$. The optimum HER activity corresponds to $\Delta G_H \cong 0$, i.e., the smallest free energy is needed for hydrogen to switch from gas state to adsorbed state or *vice versa*.[39] Figure 2a shows ΔG_H for different hydrogen coverage C_H (defined as number of H* per surface area). While ΔG_H increases monotonically with C_H for MoC-G and MoC-SW because of repulsive H–H interactions, ΔG_H oscillates at low C_H for MoC-MV and MoC-DV because of mesomeric effect and compensation of dangling bonds. The mesomeric effect is caused by hydrogen adsorption that breaks graphene π bonds and delocalizes the electrons of H* at neighboring sites (ortho or para sites). These sites then become favored sites for subsequent hydrogen adsorption.[40]

To determine the hydrogen coverage under different electrochemical environments, we compute the total hydrogen adsorption free energy ΔG_{tot} with considerations of pH and external potential U (see the Supporting Information).[41] Figure 2b shows ΔG_{tot} of the four coupled systems; the most favored C_H has the lowest ΔG_{tot}, and the corresponding ΔG_H for different C_H is shown in Figure 2a. On MoC-G, H* interacts weakly with the surface (ΔG_H = 0.21 eV) at C_H = 1.15 H*/nm^2 from 0 to −0.3 V. In contrast, hydrogen adsorption is stronger on MoC-SW and MoC-MV at 1.15 H*/nm^2 (ΔG_H = −0.27 eV) and 2.30 H*/nm^2 (ΔG_H = −0.32 eV) below −0.1 V, respectively. Surprisingly, MoC-DV is predicted to have a strong HER activity (ΔG_H = −0.14 eV) at 5.76 H*/nm^2 with only a small overpotential of −0.05 V. This will be also validated by examining the exchange current density, as will be discussed later.

The overall HER reaction $H^+ + e^- \rightarrow \frac{1}{2}H_2$ takes place via two possible pathways, namely, the Volmer–Heyrovsky or the Volmer–Tafel. In an acidic solution, the three elementary steps can be written as

$$H_3O^+ + e^- \leftrightarrow H^* + H_2O \quad \text{(Volmer)}$$

$$H_3O^+ + e^- + H^* \leftrightarrow H_2O + H_2 \quad \text{(Heyrovsky)}$$

$$H^* + H^* \leftrightarrow H_2 \quad \text{(Tafel)}$$

https://dx.doi.org/10.1021/acs.jpclett.0c00615
J. Phys. Chem. Lett. 2020, 11, 2759−2764

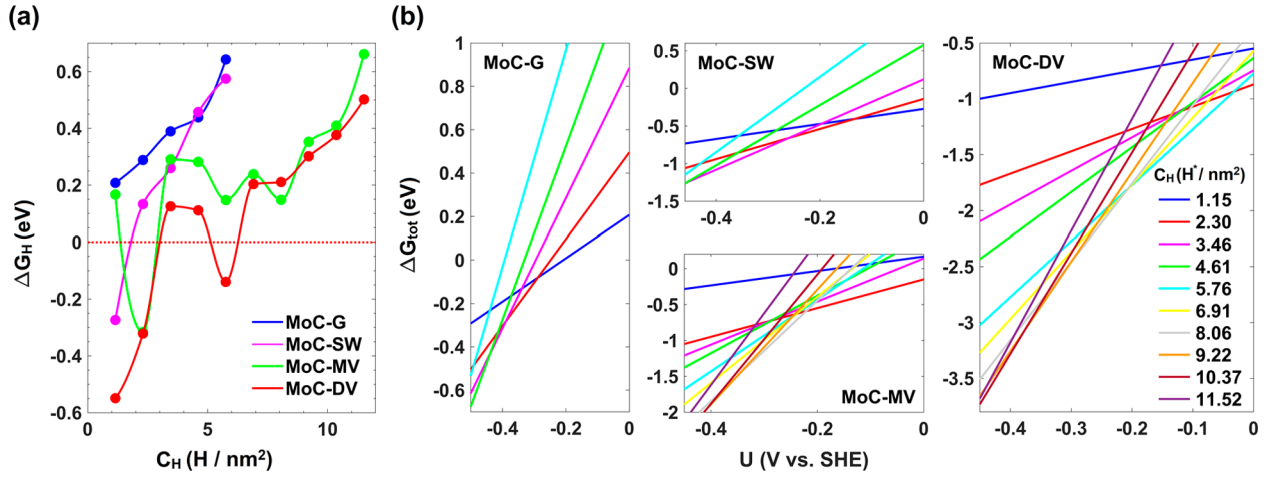

Figure 2. (a) Hydrogen adsorption free energy, ΔG_H, as a function of hydrogen coverage, C_H. The red-dashed line indicates $\Delta G_H = 0$ for the optimum HER rate. (b) Total hydrogen adsorption free energy, ΔG_{tot}, as a function of external potential, U, at different hydrogen coverages, C_H. See Figure S2 for 3D representations of the adsorption configurations near 0 vs SHE. For panels a and b, we show only the values at the hydrogen coverages that are relevant to the HER potential window from 0 to −0.5 V vs SHE.

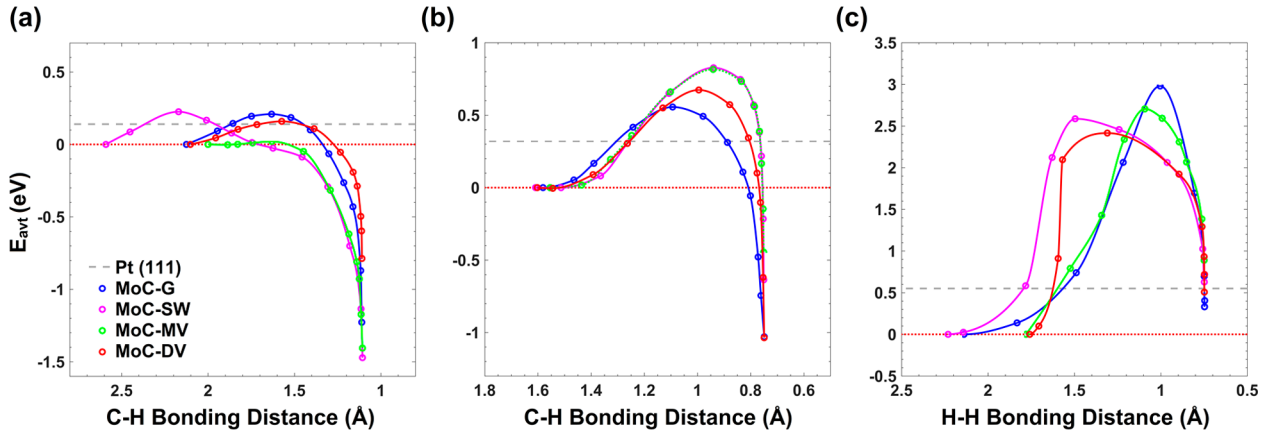

Figure 3. Minimum-energy pathways for the (a) Volmer, (b) Heyrovsky, and (c) Tafel reactions. The reaction pathway is gauged using the bonding distance between C and H in panels a and b or the distance between two hydrogen atoms that are involved in the formation of H_2 in panel c. The hydrogen coverage for each reaction is selected at $U = -0.05$ V, as shown in Figure 2b. The dots indicate the images employed in the NEB simulations.

The Volmer reaction refers to hydrogen deposition from liquid water to the surface. To form H_2(g), H* can react either with H^+ in solution through the Heyrovsky reaction or with another H* on the surface through the Tafel reaction. Figure 3 shows that the Volmer−Heyrovsky pathway is preferred for all structures with an activation barrier E_{avt} less than 0.3 eV for the Volmer reaction and 0.9 eV for the Heyrovsky reaction. Thus, the Heyrovsky reaction is the rate-determining step (rds). In contrast, the Volmer−Tafel pathway is hindered by the large activation barriers (E_{avt} > 2.4 eV) of the Tafel reaction. For comparison, we also show the corresponding activation barriers on Pt (111) where both of the Volmer−Heyrovsky and the Volmer−Tafel pathways are accessible with E_{avt} less than ∼0.7 eV.[42] We also use an extrapolation scheme[43,44] to eliminate finite-size effect for reaction energy and activation energy, but our conclusions did not change that the Volmer−Heyrovsky is the favorable route with the Heyrovsky reaction as the rds for all systems (see the Supporting Information for calculation details and Table S2 for the corrected E_{avt}).

The overall HER with the Heyrovsky reaction as the rds can be described from the current−potential[45]

$$j = nFk_0C_{tot}\theta \exp(-\beta f\eta) \quad (2)$$

where $f = F/RT$ with F Faraday's constant and R the gas constant; the temperature T is chosen to be room temperature (298 K). n is the total electrons involved per active site, and k_0 is the rate constant. C_{tot} is the concentration of H* and H^+ near the electrode, which is approximated as the number of active sites per surface area. The overpotential $\eta = U - U_{SHE}$ is the difference between the external potential, U, and the equilibrium potential, U_{SHE}, that is theoretically defined as 0 V vs standard hydrogen electrode (SHE). The symmetry factor β is defined as the fraction of the activation barrier induced by the overpotential η.[46,47] For each γ-MoC supported graphene system, we compute β by evaluating the change of excess charge between transition and initial states using Bader analysis, as suggested by Chan et al.[43] See the Supporting Information and Table S2. We find that $\beta = 0.1-0.35$. $\beta < 0.5$ indicates that the transition state of a reaction is final-state-like rather than initial-state-like.[47] Thus, for the coupled systems, the transition states are final-state-like, as can be also verified from examining the C−H bond length shown in Figure 3(b).

https://dx.doi.org/10.1021/acs.jpclett.0c00615
J. Phys. Chem. Lett. 2020, 11, 2759−2764

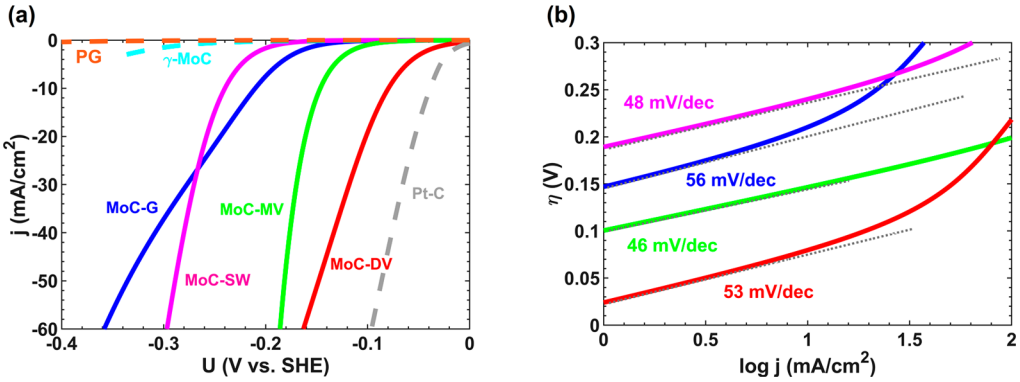

Figure 4. (a) Polarization curves for γ-MoC supported graphene systems. For comparison, we show experimental Pt−C from ref 15, as well as computed currents for isolated γ-MoC from ref 4 and pure graphene (PG) from ref 49. The computed curves are obtained using eqs 2 and 3 with k_0 = 200 site^{-1} s^{-1}. (b) Tafel slopes of the corresponding γ-MoC supported graphene systems in panel a.

Near the electrode surface, the fraction of hydrogen atoms that are involved in HER can be written as

$$\theta = \begin{cases} \dfrac{1}{K_V \exp(\eta f) + 1} & \text{for } \Delta G_H < 0 \\ \dfrac{K_V}{\exp(\eta f) + K_V} & \text{for } \Delta G_H > 0 \end{cases} \quad (3)$$

where $K_V = \exp(-\Delta G_H/k_B T)$ with the averaged ΔG_H among all adsorption sites corresponding to the hydrogen coverage near zero overpotential (see the detailed discussion for ΔG_H and the derivation of θ in the Supporting Information).[39] For η = 0, θ is of the form of a Langmuir model that has been applied widely to study HER on various catalytists.[39,45,48] θ rapidly increases with η attaining 1 when η is negatively away from 0. Thus, as expected, more hydrogen atoms are involved in HER at negative potentials that can be understood from the enhanced stabilization of H^+ on electrode surface with negative potential. This behavior of θ is also consistent with the trend of increasing C_H with negative potential from the *ab initio* thermodynamics results in Figure 2b. Furthermore, H^+ that comes to the surface at higher C_H is more likely to form H_2 as can be seen from Figure 2a that ΔG_H increases with increasing C_H. Note that ΔG_H is an intrinsic property that is independent of η as defined in eq S3.

The rate constant $k_0 \approx 200$ site^{-1} s^{-1} is universal for ideal HER catalysts.[39] To validate that this value of k_0 is also applicable on the Mo_xC supported graphene systems, we fit eq 2 to various experimental currents on similar systems (see the Supporting Information). We find excellent fits with k_0 from 162 to 383 site^{-1}s^{-1}. The obtained range for k_0 is consistent with the previous estimate of ∼200 site^{-1} s^{-1} on transition metals and β-Mo_2C surfaces.[35,39] In addition, the curvature of the experimental currents corresponds to β = 0.3−0.4, which is in good agreement with our computed values from DFT β = 0.1−0.35 for the different γ-MoC supported graphene systems.

Figure 4a depicts the HER polarization curves from eqs 2 and 3. For comparison, we also reproduce the curves of isolated pure graphene, γ-MoC bulk, and 20 wt % Pt on carbon black (Pt−C) obtained from experiments.[4,15,49] We show clearly that the coupling of γ-MoC and graphene enhances the HER activity, which are sluggish on graphene or γ-MoC bulk in their isolated form. Further, the presence of graphene defect chemistry modulates the HER activities of the coupled systems: MoC-SW shows a similar HER activity with MoC-G, whereas MoC-MV and MoC-DV display enhanced activities. Using eqs 2 and 3, we calculate the exchange current densities, j_0, at zero external potential; these are reported in the Supporting Information. The MoC-DV has the highest j_0 of ∼1 × 10^{-4} A/cm^2 that is comparable to the optimum HER catalysts.[39]

To further compare with experimental studies, we measure the Tafel slopes $d\eta/d\log(j)$, which is often used to determine the HER mechanism. Figure 4b shows the Tafel slopes as obtained numerically from the currents in Figure 4a or in a closed form $d\eta/d\log(j) = -2.303RT/F(1 + \beta)$ that can be derived from eqs 2 and 3. As seen from the figure, the Tafel slope ranges from 45 to 53 mV/dec^{-1} for the γ-MoC supported graphene systems, suggesting that the Heyrovsky reaction is the rds.[50] This corroborates the NEB calculations. It should be noted that even though there is debate in the literature on whether the Tafel slope can be evaluated using $d\eta/d\log(j) = -2.303RT/F(1 + \beta)$,[51] such an expression follows from the exchange current model of eq 2 that is a very good fit to experimental results as discussed before.

Experimentally, enhanced HER activities have been reported on several graphene-coated Mo_xC catalysts with nitrogen- or phosphorus-doped graphene or reduced graphene oxide.[15,26,52,53] Our study shows that the optimization of these catalysts requires a fine-tuning between Mo_xC supports and graphene bonding chemistry. Such interplay between both effects ultimately would stabilize hydrogen on graphene that is otherwise inert. The underpinning of this stabilization is due to the charge-transfer effect. Extra electrons (holes) on graphene will occupy graphene's antibonding π^* (bonding π) bands, which weakens graphene π bonding and increases hydrogen stabilization as less energy is required to break the graphene π bonds.[53,54] While Mo_xC in previous experiments belonged to different phases such as Mo_2C (JCPDS 15-0457,[15] 65-8766,[52] and 01-079-0744[55]) and MoC (PDF 65-3558),[26] and graphene is modified in different ways, there are two main factors that makes our findings general. First, charge donation from Mo_xC to graphene is expected to be from Mo irrespective of Mo_xC phase, as carbon-terminated surfaces are not favorable with graphene. Second, the doping nature of graphene can be characterized by charge buildup or depletion irrespective of the defect chemistry, which directly impacts the bonding of the hydrogen adsorbates.[56,57] These factors explain why our results on γ-MoC supported graphene are similar to experimental results on graphene-coated Mo_xC catalysts[13,26,52] in terms of displaying similar HER exchange rates 1 × 10^{-4} A/cm^2 and in

https://dx.doi.org/10.1021/acs.jpclett.0c00615
J. Phys. Chem. Lett. 2020, 11, 2759−2764

having the Volmer−Heyrovsky as preferred HER mechanism with the Heyrovsky reaction as rds.

Using first-principles calculations, we have investigated the HER on γ-phase MoC supported graphene with graphene defects including Stone−Wales, monovacancies, and divacancies. We show that the reaction processes take place via the fast-rate Volmer reaction followed by the Heyrovsky reaction as the rate-limiting step, while the Tafel reaction experiences high activation barrier over 2 eV. We have used a computational approach to obtain electrochemical linear sweep voltammetry and to quantify the overall HER rate using kinetic and thermodynamic variables obtained from first-principles calculations. We show that the supported γ-phase MoC and divacancy defects play a role to modulate the hydrogen adsorption events resulting in an exchange current density of 1×10^{-4} A/cm^2. This study provides atomistic insights on general graphene-coated Mo_xC electrocatalysts.

■ ASSOCIATED CONTENT

Supporting Information

The Supporting Information is available free of charge at https://pubs.acs.org/doi/10.1021/acs.jpclett.0c00615.

Computational approach and details; atomic structure models; adhesion energy; hydrogen adsorption and free energies; NEB calculations of reaction pathways with extrapolation; derivation of thermodynamic exchange current model; fitting of k_0 to experimental measurements; derivation of Tafel slope (PDF)

■ AUTHOR INFORMATION

Corresponding Author

Wissam A. Saidi − *Department of Materials Science and Engineering, University of Pittsburgh, Pittsburgh, Pennsylvania 15260, United States;* orcid.org/0000-0001-6714-4832; Email: alsaidi@pitt.edu

Author

Timothy T. Yang − *Department of Materials Science and Engineering, University of Pittsburgh, Pittsburgh, Pennsylvania 15260, United States*

Complete contact information is available at: https://pubs.acs.org/10.1021/acs.jpclett.0c00615

Notes

The authors declare no competing financial interest.

■ ACKNOWLEDGMENTS

We acknowledge a start-up fund from the department of Mechanical Engineering and Materials Science at the University of Pittsburgh and partial support from National Science Foundation (DMR-1809085). We are grateful for computing time provided by CRC resources at the University of Pittsburgh, Extreme Science and Engineering Discovery Environment (XSEDE) supported by the National Science Foundation (NSF OCI-1053575), and by Argonne Leadership Computing Facility, which is a DOE Office of Science User Facility supported under Contract DE-AC02-06CH11357.

■ REFERENCES

(1) Bockris, J. O. M.; Ammar, I. A.; Huq, A. K. M. S. The Mechanism of the Hydrogen Evolution Reaction on Platinum, Silver and Tungsten surfaces in Acid Solutions. *J. Phys. Chem.* **1957**, *61*, 879−886.

(2) Yang, T. T.; Tan, T. L.; Saidi, W. A. High Activity toward the Hydrogen Evolution Reaction on the Edges of MoS2-Supported Platinum Nanoclusters Using Cluster Expansion and Electrochemical Modeling. *Chem. Mater.* **2020**, *32*, 1315−1321.

(3) Lu, J.; Hugosson, H.; Eriksson, O.; Nordstrom, L.; Jansson, U. Chemical vapour deposition of molybdenum carbides: aspects of phase stability. *Thin Solid Films* **2000**, *370*, 203−212.

(4) Wan, C.; Regmi, Y. N.; Leonard, B. M. Multiple phases of molybdenum carbide as electrocatalysts for the hydrogen evolution reaction. *Angew. Chem., Int. Ed.* **2014**, *53*, 6407−10.

(5) Liao, L.; Wang, S.; Xiao, J.; Bian, X.; Zhang, Y.; Scanlon, M. D.; Hu, X.; Tang, Y.; Liu, B.; Girault, H. H. A nanoporous molybdenum carbide nanowire as an electrocatalyst for hydrogen evolution reaction. *Energy Environ. Sci.* **2014**, *7*, 387−392.

(6) Chen, J.; Zhou, W.; Jia, J.; Wan, B.; Lu, J.; Xiong, T.; Tong, Q.; Chen, S. Porous molybdenum carbide microspheres as efficient binder-free electrocatalysts for suspended hydrogen evolution reaction. *Int. J. Hydrogen Energy* **2017**, *42*, 6448−6454.

(7) Meng, T.; Zheng, L.; Qin, J.; Zhao, D.; Cao, M. A three-dimensional hierarchically porous Mo2C architecture: salt-template synthesis of a robust electrocatalyst and anode material towards the hydrogen evolution reaction and lithium storage. *J. Mater. Chem. A* **2017**, *5*, 20228−20238.

(8) Wu, H. B.; Xia, B. Y.; Yu, L.; Yu, X. Y.; Lou, X. W. Porous molybdenum carbide nano-octahedrons synthesized via confined carburization in metal-organic frameworks for efficient hydrogen production. *Nat. Commun.* **2015**, *6*, 6512.

(9) Deng, Y.; Mou, J.; Wu, H.; Zhou, L.; Zheng, Q.; Lam, K. H.; Xu, C.; Lin, D. Enhanced Electrochemical Performance in Ni-Doped $LiMn_2O_4$-Based Composite Cathodes for Lithium-Ion Batteries. *ChemElectroChem* **2017**, *4* (6), 1362−1371.

(10) Politi, J. R.; Vines, F.; Rodriguez, J. A.; Illas, F. Atomic and electronic structure of molybdenum carbide phases: bulk and low Miller-index surfaces. *Phys. Chem. Chem. Phys.* **2013**, *15*, 12617−25.

(11) Kitchin, J. R.; Nørskov, J. K.; Barteau, M. A.; Chen, J. G. Trends in the chemical properties of early transition metal carbide surfaces: A density functional study. *Catal. Today* **2005**, *105*, 66−73.

(12) Liu, Y.; Yu, G.; Li, G. D.; Sun, Y.; Asefa, T.; Chen, W.; Zou, X. Coupling Mo2 C with Nitrogen-Rich Nanocarbon Leads to Efficient Hydrogen-Evolution Electrocatalytic Sites. *Angew. Chem., Int. Ed.* **2015**, *54*, 10752−7.

(13) Ma, R.; Zhou, Y.; Chen, Y.; Li, P.; Liu, Q.; Wang, J. Ultrafine Molybdenum Carbide Nanoparticles Composited with Carbon as a Highly Active Hydrogen-Evolution Electrocatalyst. *Angew. Chem., Int. Ed.* **2015**, *54*, 14723−7.

(14) Pan, L. F.; Li, Y. H.; Yang, S.; Liu, P. F.; Yu, M. Q.; Yang, H. G. Molybdenum carbide stabilized on graphene with high electrocatalytic activity for hydrogen evolution reaction. *Chem. Commun. (Cambridge, U. K.)* **2014**, *50*, 13135−7.

(15) Li, J. S.; Wang, Y.; Liu, C. H.; Li, S. L.; Wang, Y. G.; Dong, L. Z.; Dai, Z. H.; Li, Y. F.; Lan, Y. Q. Coupled molybdenum carbide and reduced graphene oxide electrocatalysts for efficient hydrogen evolution. *Nat. Commun.* **2016**, *7*, 11204.

(16) Huang, Y.; Gong, Q.; Song, X.; Feng, K.; Nie, K.; Zhao, F.; Wang, Y.; Zeng, M.; Zhong, J.; Li, Y. Mo2C Nanoparticles Dispersed on Hierarchical Carbon Microflowers for Efficient Electrocatalytic Hydrogen Evolution. *ACS Nano* **2016**, *10*, 11337−11343.

(17) Youn, D. H.; Han, S.; Kim, J. Y.; Kim, J. Y.; Park, H.; Choi, S. H.; Lee, J. S. Highly Active and Stable Hydrogen Evolution Electrocatalysts Based on Molybdenum Compounds on Carbon Nanotube Graphene Hybrid Support. *ACS Nano* **2014**, *8*, 5164−5173.

(18) Zhang, K.; Zhao, Y.; Fu, D.; Chen, Y. Molybdenum carbide nanocrystal embedded N-doped carbon nanotubes as electrocatalysts for hydrogen generation. *J. Mater. Chem. A* **2015**, *3*, 5783−5788.

(19) Tsai, C.; Abild-Pedersen, F.; Nørskov, J. K. Tuning the MoS2 Edge-Site Activity for Hydrogen Evolution via Support Interactions. *Nano Lett.* **2014**, *14*, 1381.
(20) Wang, J.; Xia, H.; Peng, Z.; Lv, C.; Jin, L.; Zhao, Y.; Huang, Z.; Zhang, C. Graphene Porous Foam Loaded with Molybdenum Carbide Nanoparticulate Electrocatalyst for Effective Hydrogen Generation. *ChemSusChem* **2016**, *9*, 855−62.
(21) Geim, A. K.; Grigorieva, I. V. Van der Waals heterostructures. *Nature* **2013**, *499*, 419−25.
(22) Ge, L.; Yuan, H.; Min, Y.; Li, L.; Chen, S.; Xu, L.; Goddard, W. A. Predicted Optimal Bifunctional Electrocatalysts for the Hydrogen Evolution Reaction and the Oxygen Evolution Reaction Using Chalcogenide Heterostructures Based on Machine Learning Analysis of in Silico Quantum Mechanics Based High Throughput Screening. *J. Phys. Chem. Lett.* **2020**, *11*, 869−876.
(23) Wu, C.; Li, D.; Ding, S.; Rehman, Z. u.; Liu, Q.; Chen, S.; Zhang, B.; Song, L. Monoatomic Platinum-Anchored Metallic MoS2: Correlation between Surface Dopant and Hydrogen Evolution. *J. Phys. Chem. Lett.* **2019**, *10*, 6081−6087.
(24) Zheng, Y.; Jiao, Y.; Zhu, Y.; Li, L. H.; Han, Y.; Chen, Y.; Du, A.; Jaroniec, M.; Qiao, S. Z. *Nat. Commun.* **2014**, *5*, 3783.
(25) Biroju, R. K.; Das, D.; Sharma, R.; Pal, S.; Mawlong, L. P. L.; Bhorkar, K.; Giri, P. K.; Singh, A. K.; Narayanan, T. N. Hydrogen Evolution Reaction Activity of Graphene−MoS2 van der Waals Heterostructures. *ACS Energy Letters* **2017**, *2*, 1355−1361.
(26) Yang, X.; Feng, X.; Tan, H.; Zang, H.; Wang, X.; Wang, Y.; Wang, E.; Li, Y. N-Doped graphene-coated molybdenum carbide nanoparticles as highly efficient electrocatalysts for the hydrogen evolution reaction. *J. Mater. Chem. A* **2016**, *4*, 3947−3954.
(27) Kresse, G.; Hafner, J. Ab initio molecular dynamics for liquid metals. *Phys. Rev. B: Condens. Matter Mater. Phys.* **1993**, *47* (1), 558−561.
(28) Kresse, G.; Hafner, J. Ab-initio molecular-dynamics simulation of the liquid-metal amorphous-semiconductor transition in germanium. *Phys. Rev. B: Condens. Matter Mater. Phys.* **1994**, *49*, 14251−14269.
(29) Perdew, J. P.; Burke, K.; Ernzerhof, M. Generalized Gradient Approximation Made Simple. *Phys. Rev. Lett.* **1996**, *77*, 3865.
(30) Tkatchenko, A.; Scheffler, M. Accurate Molecular Van Der Waals Interactions from Ground-State Electron Density and Free-Atom Reference Data. *Phys. Rev. Lett.* **2009**, *102*, 073005.
(31) Al-Saidi, W.; Voora, V. K.; Jordan, K. D. An assessment of the vdW-TS method for extended systems. *J. Chem. Theory Comput.* **2012**, *8*, 1503−1513.
(32) Zur, A.; McGill, T. C. Lattice match: An application to heteroepitaxy. *J. Appl. Phys.* **1984**, *55*, 378−386.
(33) Vines, F.; Sousa, C.; Liu, P.; Rodriguez, J. A.; Illas, F. A systematic density functional theory study of the electronic structure of bulk and (001) surface of transition-metals carbides. *J. Chem. Phys.* **2005**, *122*, 174709.
(34) Tian, W.; Li, W.; Yu, W.; Liu, X. A Review on Lattice Defects in Graphene: Types, Generation, Effects and Regulation. *Micromachines* **2017**, *8*, 163.
(35) Yang, T. T.; Saidi, W. A. Tuning the hydrogen evolution activity of beta-Mo2C nanoparticles via control of their growth conditions. *Nanoscale* **2017**, *9*, 3252−3260.
(36) Goler, S.; Coletti, C.; Tozzini, V.; Piazza, V.; Mashoff, T.; Beltram, F.; Pellegrini, V.; Heun, S. Influence of Graphene Curvature on Hydrogen Adsorption: Toward Hydrogen Storage Devices. *J. Phys. Chem. C* **2013**, *117*, 11506−11513.
(37) Pan, H. Waved graphene: Unique structure for the adsorption of small molecules. *Mater. Chem. Phys.* **2017**, *189*, 111−117.
(38) Tada, K.; Furuya, S.; Watanabe, K. Ab initio study of hydrogen adsorption to single-walled carbon nanotubes. *Phys. Rev. B: Condens. Matter Mater. Phys.* **2001**, *63*, 155405.
(39) Nørskov, J. K.; Bligaard, T.; Logadottir, A.; Kitchin, J. R.; Chen, J. G.; Pandelov, S.; Stimming, U. Trends in the Exchange Current for Hydrogen Evolution. *J. Electrochem. Soc.* **2005**, *152*, J23.
(40) Hornekaer, L.; Rauls, E.; Xu, W.; Sljivancanin, Z.; Otero, R.; Stensgaard, I.; Laegsgaard, E.; Hammer, B.; Besenbacher, F. Clustering of chemisorbed H(D) atoms on the graphite (0001) surface due to preferential sticking. *Phys. Rev. Lett.* **2006**, *97*, 186102.
(41) Saidi, W. A. Oxygen Reduction Electrocatalysis Using N-Doped Graphene Quantum-Dots. *J. Phys. Chem. Lett.* **2013**, *4*, 4160−4165.
(42) Skulason, E.; Karlberg, G. S.; Rossmeisl, J.; Bligaard, T.; Greeley, J.; Jonsson, H.; Norskov, J. K. Density functional theory calculations for the hydrogen evolution reaction in an electrochemical double layer on the Pt(111) electrode. *Phys. Chem. Chem. Phys.* **2007**, *9*, 3241−50.
(43) Chan, K.; Norskov, J. K. Potential Dependence of Electrochemical Barriers from ab Initio Calculations. *J. Phys. Chem. Lett.* **2016**, *7*, 1686−90.
(44) Chan, K.; Norskov, J. K. Electrochemical Barriers Made Simple. *J. Phys. Chem. Lett.* **2015**, *6*, 2663−8.
(45) Shinagawa, T.; Garcia-Esparza, A. T.; Takanabe, K. Insight on Tafel slopes from a microkinetic analysis of aqueous electrocatalysis for energy conversion. *Sci. Rep.* **2015**, *5*, 13801.
(46) Butler, J. A. V. Studies in heterogeneous equilibria. Part II.—The kinetic interpretation of the nernst theory of electromotive force. *Trans. Faraday Soc.* **1924**, *19*, 729−733.
(47) Bard, A. J.; Faulkner, L. R. *Electrochemical Method*; John Wiley & Sons, Inc., 2001; Vol. 2.
(48) Skúlason, E.; Tripkovic, V.; Björketun, M. E.; Gudmundsdóttir, S.; Karlberg, G.; Rossmeisl, J.; Bligaard, T.; Jónsson, H.; Nørskov, J. K. Modeling the Electrochemical Hydrogen Oxidation and Evolution Reactions on the Basis of Density Functional Theory Calculations. *J. Phys. Chem. C* **2010**, *114*, 18182−18197.
(49) Tian, Y.; Wei, Z.; Wang, X.; Peng, S.; Zhang, X.; Liu, W.-m. Plasma-etched, S-doped graphene for effective hydrogen evolution reaction. *Int. J. Hydrogen Energy* **2017**, *42*, 4184−4192.
(50) Li, Y.; Wang, H.; Xie, L.; Liang, Y.; Hong, G.; Dai, H. MoS2 nanoparticles grown on graphene: an advanced catalyst for the hydrogen evolution reaction. *J. Am. Chem. Soc.* **2011**, *133*, 7296−9.
(51) Guidelli, R.; Compton, R. G.; Feliu, J. M.; Gileadi, E.; Lipkowski, J.; Schmickler, W.; Trasatti, S. Defining the transfer coefficient in electrochemistry: An assessment (IUPAC Technical Report). *Pure Appl. Chem.* **2014**, *86*, 245−258.
(52) Wei, H.; Xi, Q.; Chen, X.; Guo, D.; Ding, F.; Yang, Z.; Wang, S.; Li, J.; Huang, S. Molybdenum Carbide Nanoparticles Coated into the Graphene Wrapping N-Doped Porous Carbon Microspheres for Highly Efficient Electrocatalytic Hydrogen Evolution Both in Acidic and Alkaline Media. *Adv. Sci. (Weinh)* **2018**, *5*, 1700733.
(53) Pizzochero, M.; Leenaerts, O.; Partoens, B.; Martinazzo, R.; Peeters, F. M. Hydrogen adsorption on nitrogen and boron doped graphene. *J. Phys.: Condens. Matter* **2015**, *27*, 425502.
(54) Huang, L. F.; Ni, M. Y.; Zhang, G. R.; Zhou, W. H.; Li, Y. G.; Zheng, X. H.; Zeng, Z. Modulation of the thermodynamic, kinetic, and magnetic properties of the hydrogen monomer on graphene by charge doping. *J. Chem. Phys.* **2011**, *135* (6), 064705.
(55) Tuomi, S.; Guil-Lopez, R.; Kallio, T. Molybdenum carbide nanoparticles as a catalyst for the hydrogen evolution reaction and the effect of pH. *J. Catal.* **2016**, *334*, 102−109.
(56) Gong, P. L.; Huang, L. F.; Zheng, X. H.; Zhang, Y. S.; Zeng, Z. Nonlocal and Local Electrochemical Effects of Doping Impurities on the Reactivity of Graphene. *J. Phys. Chem. C* **2015**, *119* (19), 10513−10519.
(57) Wang, L.; Sofer, Z.; Pumera, M. Will Any Crap We Put into Graphene Increase Its Electrocatalytic Effect? *ACS Nano* **2020**, *14* (1), 21−25.

https://dx.doi.org/10.1021/acs.jpclett.0c00615
J. Phys. Chem. Lett. 2020, 11, 2759−2764